Proceedings RootS25
3rd International Workshop on Soil-Vegetation-Atmosphere Interaction
Boldrin D, Cecconi M, Cotecchia F, Leung A, Pedone G, Perrini P, Romero E, Tagarelli V, Zdravković L (eds)
ISSN: 3107-300X

doi: doi.org/10.53243/RootS2025-8

Numerical modelling of soil moisture variations beneath residential buildings due to soil–vegetation–atmosphere interaction

M. Haddad[1*], D. Do[1], Y. Jin[1], D. Hoxha[1], L. Ighil Ameur[2]

[1]*Université d'Orléans, Université de Tours, INSA CVL, Laboratoire de Mécanique Gabriel Lamé (LaMé), 8 rue Léonard de Vinci, 45072 Orléans, France. * mouhcine.haddad@univ-orleans.fr*

[2]*Cerema, GéoCoD, 11 rue Laplace, 41000 Blois, France*

ABSTRACT: Seasonal climatic variations influence the moisture content of soils. In expansive clayey soils, these fluctuations can cause significant volumetric changes, leading to deformations that may compromise the stability of overlying structures. This study focuses on modelling the influence of evapotranspiration and precipitation on soil moisture dynamics beneath residential buildings, emphasizing soil–vegetation–atmosphere (SVA) interaction. The Van Genuchten–Mualem model is used to describe unsaturated water flow in the soil. Evapotranspiration is computed with the FAO Penman–Monteith equation based on realistic meteorological data. A parametric study is conducted to identify the key factors influencing soil moisture variations. Particular attention is paid to pavements, which significantly reduce moisture exchange between the soil beneath the building and the atmosphere. The study proposes a simplified yet effective numerical framework to evaluate the influence of SVA interaction on the hydraulic response of expansive soils beneath residential buildings.

Keywords: Expansive soils; Soil–vegetation–atmosphere interaction; Numerical modelling

1 INTRODUCTION

Seasonal climatic fluctuations cause cyclic variations in water content and pressure head within expansive clays, creating moisture contrasts beneath shallow foundations and inducing differential ground movements. In France, the cost of damage associated with clay shrinkage–swelling has risen significantly in recent years and is expected to continue increasing markedly in the future across the entire territory in the context of climate change (CCR, 2023). To examine these processes in a built environment, soil–vegetation–atmosphere (SVA) interactions around residential buildings are modelled in HYDRUS-2D using the Van Genuchten–Mualem model for unsaturated flow, and a Feddes water-stress function for root water uptake. A comprehensive parametric analysis explores the influence of soil hydraulic properties, vegetation parameters, climatic inputs, pavement widths, tree distances, and root-system extents to determine the dominant influences and aid in the design of mitigation approaches**.**

2 NUMERICAL MODEL

The simulations were performed with HYDRUS-2D (Šimůnek et al., 2025) over a domain 10 m deep and 20 m wide (Figure 1). A preliminary parametric study confirmed that results were not significantly influenced by widths greater than 20 m. These sensitivity tests highlighted that the finite-element mesh refined to 3 cm near the soil surface is sufficient. Adopting the symmetric hypothesis, the geometric model included half of a building with a width of 5 m and a pavement of variable width. In addition, to consider the transpiration effect an apple tree located 1.5 m from the house was chosen. Clay soil hydraulic properties were described with the Van Genuchten–Mualem model, and parameter values were adopted from (Carsel and Parrish, 1988) as listed in Table 1.

Table 1. Soil hydraulic properties used in the simulations

θ_r [−]	θ_s [−]	α [cm^{-1}]	n [−]	K_s [cm/day]	l [−]
0.068	0.38	0.008	1.09	4.8	0.5

2.1 Initial conditions

Initial conditions were generated using the model warming-up technique (Yu et al., 2019), which consists of running the model from an arbitrary initial condition for a sufficiently long period so that the influence of the initial condition becomes negligible. In our case, the simulation was initialized with a hydrostatic pressure distribution, followed by a warming-up period t_{wu} driven by historical meteorological data. Convergence was achieved for

$t_{wu} \geq 5$ years. Therefore, a spin-up duration of 5 years was adopted.

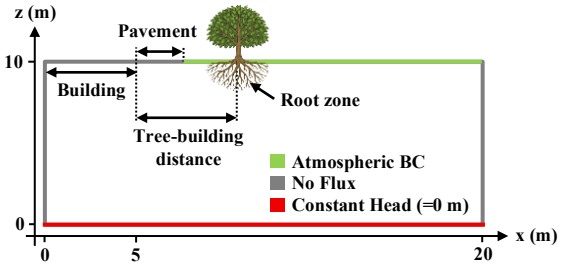

Figure 1. Model domain and boundary conditions

2.2 Meteorological inputs and boundary conditions

Meteorological data were obtained from Météo-France (Orléans station) over the period 01/01/2015–31/07/2025. The dataset included daily mean temperature (T_{mean}), mean relative humidity (RH_{mean}), wind speed at 10 m height (u_{10},), solar radiation (R_s), and precipitation (P). Missing data were gap-filled using the Villemurlin station data, located 54 km away.

Reference evapotranspiration (ET_0) was calculated using the Penman–Monteith equation (Allen et al., 1998). Potential evaporation (E_p) and potential transpiration (T_p) were derived using the dual crop coefficient approach (Allen et al., 1998).

Boundary conditions for the numerical model are shown in Figure 1. Atmospheric boundary conditions, accounting for both evaporation and precipitation, were applied at the soil surface except beneath the house and the pavement, where no-flux conditions were imposed. No-flux conditions were also specified along the lateral boundaries. At the bottom of the domain a constant pressure head of h = 0 cm was applied, representing a fixed water table at that depth.

2.3 Root water uptake

Root distribution was represented using the root model implemented in HYDRUS (Vrugt et al., 2001), with parameters taken from the literature (Nazari et al., 2021) for apple tree. Root water uptake stress was described using the Feddes model (Feddes and Zaradny, 1978), with parameters adopted from (Zheng et al., 2018) and summarized in Table 2.

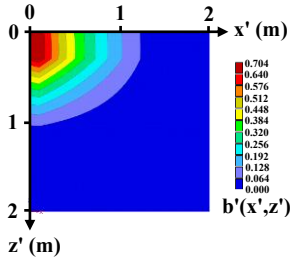

Figure 2. Root distribution used in the simulations, based on Vrugt model

Table 2. Root distribution parameters used in the simulations

Parameter	Value
X_m [cm]	150
Z_m [cm]	120
x^* [cm]	10
z^* [cm]	30
p_x [−]	1.8
p_z [−]	1.2

2.4 Soil moisture profiles and edge – center contrast

Differential settlement arises from the moisture gradient of the soil beneath the foundations. To describe this, two soil profiles were analyzed: one beneath the building edge (x = 5m) and one at the center (x = 0 m). For each profile (i) and at each time step t, the mean volumetric water content $\theta_i(t)$ was calculated. The difference between the mean moisture content of the edge and center profiles was then evaluated to quantify the moisture gradient beneath the foundations (Equation 1).

$$\delta_\theta(t) = \theta_{edge}(t) - \theta_{center}(t) \quad (1)$$

This time-dependent difference $\delta_\theta(t)$ is positive during infiltration, when wetter soil at the edge causes the greatest differential settlement from heave as $\delta_\theta(t)$ approaches its maximum $\delta_{\theta\,max}$. During dry periods the difference becomes negative, and the differential settlement from shrinkage is greatest when $\delta_\theta(t)$ reaches its minimum $\delta_{\theta\,min}$. The values of $\delta_{\theta\,max}$ and $\delta_{\theta\,min}$ were calculated over the study period (1 January 2020 to 31 July 2025). The absolute value $|\delta_{\theta\,min}|$ was used, so that a positive relative change in $|\delta_{\theta\,min}|$ indicates a stronger moisture contrast and greater potential for differential settlement during dry periods.

3 SENSITIVITY ANALYSIS

The parametric study evaluated the sensitivity of $|\delta_{\theta\,min}|$ and $|\delta_{\theta\,max}|$ considering the same variation ±20 % of each key parameter while keeping the others constant. As the reference model, we take the case of building without pavement. The tested variables included soil hydraulic properties (n, θ_s, K_s), meteorological inputs (T_{mean}, RH_{mean}, u_2, R_S, P), and vegetation parameters (S_t, the surface area associated with transpiration, and the basal crop coefficient K_{cb}). For n, the lower bound was limited to -7.33 % to satisfy $n \geq 1.01$. Likewise, RH_{mean} was increased by up to 20 % while ensuring $RH_{mean} \leq 100\%$. Figure 3 reports the outcomes as relative percentage changes of $|\delta_{\theta\,max}|$ and $|\delta_{\theta\,min}|$ with respect to the reference model.

For $|\delta_{\theta\,min}|$ (Figure 3-a), soil hydraulic parameters (n, θ_s and K_s) have the strongest influence. Under +20% perturbation, θ_s and K_s increase $|\delta_{\theta\,min}|$ by 19.82% and 8.98%, respectively, while n induces a slight decrease of −1.32%. Under −20% perturbation, θ_s and K_s decrease by −9.47% and −9.74%, and a 7.33% n decrease exhibits a large decrease (−76.49%) due to its physical lower bound. Among meteorological parameters, RH_{mean} shows a pronounced effect, with a 22.76% increase under −20% perturbation, and precipitation has a moderate impact, changing $|\delta_{\theta\,min}|$ by +15 % for −20 % and −7.14 % for +20 % perturbations. Vegetation parameters also play a quite significant role: K_{cb} affects $|\delta_{\theta\,min}|$ by about −10%, reflecting the contribution of

evapotranspiration to soil moisture contrasts. Besides, the influence of T_{mean}, R_s, u_2 and S_t is modest (<7%). In this case, increasing K_{cb} does not amplify $|\delta_{\theta\ min}|$ as one might expect. Although higher K_{cb} raises transpiration demand and reduces evaporation, transpiration is constrained by the Feddes wilting-point pressure-head threshold h_4, while evaporation is controlled by h_A, the maximum pressure head at the soil surface permitted under the prevailing soil conditions, as defined by the equilibrium between soil water and atmospheric water vapour, this value can reach much lower values than h_4. As a result, the reduction in evaporation dominates, leading to a net decrease in $|\delta_{\theta\ min}|$.

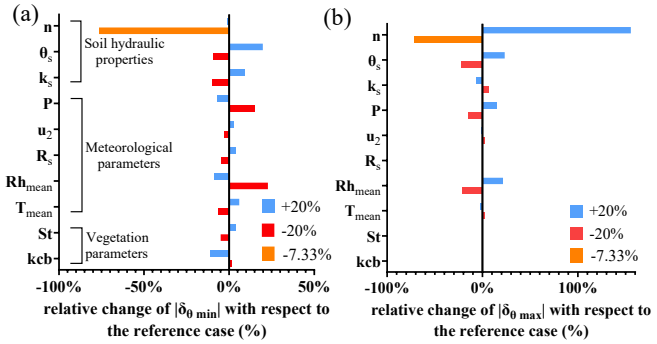

Figure 3. Sensitivity of (a) $|\delta_{\theta\ min}|$ and (b) $|\delta_{\theta\ max}|$ to ±20% parameter perturbations

For $|\delta_{\theta\ max}|$ (Figure 3-b), similar trends are observed, although some differences in magnitude appear. Soil hydraulic parameters remain highly influential: θ_s changes $|\delta_{\theta\ max}|$ by +23.24% / −22.88%, while n exhibits an exceptionally strong effect (+155.48% / −71.23%). RH_{mean} again, shows a significant effect (+21.53% / −21.45%), and precipitation (P) moderately affects $|\delta_{\theta\ max}|$ (+15.46% / −14.74%). Other meteorological and vegetation parameters have only minor influence (<3%).

These findings are in agreement with (Karunarathne et al., 2018), who reported that soil moisture at 0.3 m depth was most sensitive to the SWCC (~22 % change for a 20 % parameter variation), followed by rainfall, evaporation, hydraulic conductivity, and relative humidity, while temperature and wind speed had very limited influence.

4 INFLUENCE OF ADDITIONAL PARAMETERS

4.1 Pavement width effect

To examine the influence of a pavement (assumed to be impermeable) around the building, simulations were carried out on a model representing a building with a half-width of 5 m, a variable pavement width without tree. The results shown in Figure 4 are expressed as relative variations of $|\delta_{\theta\ max}|$ and $|\delta_{\theta\ min}|$ with respect to the reference case without pavement.

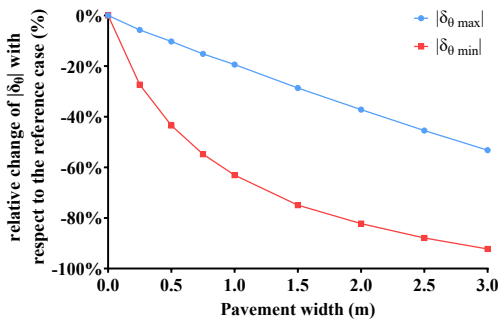

Figure 4. Relative change of $|\delta_{\theta\ min}|$ and $|\delta_{\theta\ max}|$ with pavement width

The presence of the pavement produces contrasting effects under drying and wetting conditions. For drying episodes, represented by $|\delta_{\theta\ min}|$ during periods of high evapotranspiration, the reduction is rapid for small pavement widths: a 1.5 m pavement lowers $|\delta_{\theta\ min}|$ by about 75 %. Beyond this width the effect slows, reaching roughly 92 % at 3 m. During wet periods, described by $|\delta_{\theta\ max}|$ when infiltration dominates, the response is almost linear. A pavement 1.5 m wide reduces $|\delta_{\theta\ max}|$ by 28.7 %, and a width of 3 m produces a 53.2 % reduction.

For a building without pavement, $|\delta_{\theta\ max}|$ exceeds $|\delta_{\theta\ min}|$, This indicates that edge heave during wetting is the dominant contributor to differential settlement.

Based on these results, the pavement most effectively limits drying, quickly reducing $|\delta_{\theta\ min}|$ during dry phases, but in wet periods it acts more slowly, gradually lowering the dominant wetting contrast $|\delta_{\theta\ max}|$.

4.2 Tree–building distance effect

The influence of tree proximity was assessed using a model of a building with a half-width of 5 m, no pavement, and a tree placed at varying distances from the house. Figure 5 shows the relative changes in $|\delta_{\theta\ max}|$ and $|\delta_{\theta\ min}|$ compared with a reference model without the tree.

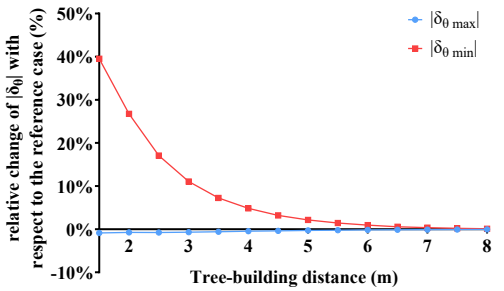

Figure 5. Relative change of $|\delta_{\theta\ min}|$ and $|\delta_{\theta\ max}|$ with tree-building distance

The presence of the tree primarily affects $|\delta_{\theta min}|$, consistent with its control by evapotranspiration. When the tree is far from the building (8 m), results are nearly identical to the reference case. As the tree moves closer, $|\delta_{\theta min}|$ rises progressively: +4.8 % at 4 m, +11.1 % at 3 m, +26.8 % at 2 m, and +39.5 % at 1.5 m. In contrast,

the effect on $|\delta_{\theta max}|$ (wetting) remains very small, below -1 %. These trends reflect the specific root distribution and water-stress parameters used in this study, different assumptions for root architecture or stress response could modify the magnitude of the tree's influence.

4.3 Root distribution effect

The influence of root distribution was examined using a model of a building with a half-width of 5 m, no pavement, and a tree located 1.5 m from the building. Several simulations were performed with different maximum horizontal and vertical rooting extents (X_m and Z_m). Results in Figure 6 show the relative changes of $|\delta_{\theta\ max}|$ and $|\delta_{\theta\ min}|$ compared with a reference case of X_m= 100 cm and Z_m= 100 cm.

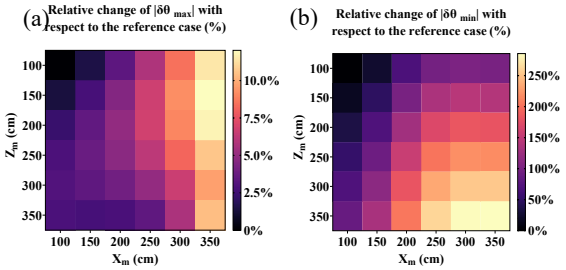

Figure 6. Effect of horizontal Xm and vertical Zm root extent on the relative change of (a) $|\delta_{\theta max}|$ and (b) $|\delta_{\theta min}|$

For $|\delta_{\theta\ max}|$ (wetting, Figure 6-a), the horizontal extent X_m exerts the greatest influence: larger X_m values increase $|\delta_{\theta\ max}|$, because more roots extend beneath the building, lowering the center profile moisture and enhancing the edge–center gap during infiltration. This effect remains modest, with a maximum variation of about +12 %.

In contrast, the impact on $|\delta_{\theta\ min}|$ (drying, Figure 6-b) is much stronger. Both X_m and Z_m contribute similarly to increasing $|\delta_{\theta\ min}|$, reaching up to +286 % when X_m= 350 cm and Z_m= 350 cm. In terms of pressure head, this case produces $|\delta_{h\ min}|$ = 2393.94 cm, far exceeding $|\delta_{h\ max}|$ = 334.36 cm. For the reference configuration (X_m= 100, Z_m= 100 cm), the opposite relationship holds ($|\delta_{h\ min}| < |\delta_{h\ max}|$).

These results highlight that, depending on the assumed root distribution, drought-driven contrasts can dominate the hydraulic differential beneath the building. Different parameterizations of root distribution could therefore significantly alter the predicted influence of vegetation.

5 CONCLUSIONS

The results highlight the dominant influence of soil hydraulic parameters, with relative humidity and precipitation emerging as the most significant meteorological factors on the soil moisture variations beneath residential buildings. Pavement significantly mitigates drying-induced moisture contrasts. Tree proximity predominantly intensifies drying, and extensive root systems can even reverse the dominant pattern of differential settlement.

These outcomes underscore the need for precise characterisation of the soil water-retention curve and hydraulic conductivity, the implementation of moderate pavement widths to mitigate shrinkage, and the judicious placement of vegetation near façades. This work will be extended and completed through hydro-mechanical coupling to achieve a more robust assessment of differential settlement.

6 ACKNOWLEDGEMENTS

This research was conducted as part of the SAFE RGA project (Innovative Solutions for Adapting Buildings Exposed to Drought Facing the Expansion of the Clay Shrinkage–Swelling Phenomenon), funded by ADEME (French Agency for Ecological Transition).

7 REFERENCES

Carsel, R.F., Parrish, R.S. 1988. Developing joint probability distributions of soil water retention characteristics, *Water Resour. Res.* **24**, 755–769.

CCR. 2023. *Conséquences du changement climatique sur le coût des catastrophes naturelles en France à horizon 2050 - 2023*. CCR, Réassureur Public.

Feddes, R.A., Zaradny, H. 1978. Model for simulating soil-water content considering evapotranspiration — Comments, *J. Hydrol* **37**, 393–397.

Karunarathne, A.M.A.N., Fardipour, M., Gad, E.F., Rajeev, P., Disfani, M.M., Sivanerupan, S., Wilson, J.L. 2018. Modelling of Climate Induced Moisture Variations and Subsequent Ground Movements in Expansive Soils, *Geotech. Geol. Eng.* **36**, 2455–2477.

Nazari, E., Besharat, S., Zeinalzadeh, K., Mohammadi, A. 2021. Measurement and simulation of the water flow and root uptake in soil under subsurface drip irrigation of apple tree, *Agric. Water Manag.* **255**, 106972.

Šimůnek, J., van Genuchten, M., Šejna, M. 2025. *The HYDRUS Software Package for Simulating One-, Two-, and Three-Dimensional Movement of Water, Heat, and Multiple Solutes in Variably Saturated Porous Media, Technical Manual II, Hydrus (2D/3D), Version 5.04*. PC Progress, Prague, Czech republic.

Vrugt, J.A., van Wijk, M.T., Hopmans, J.W., Šimunek, J. 2001. One-, two-, and three-dimensional root water uptake functions for transient modeling, *Water Resour. Res* **37**, 2457–2470.

Yu, D., Yang, J., Shi, L., Zhang, Q., Huang, K., Fang, Y., Zha, Y. 2019. On the uncertainty of initial condition and initialization approaches in variably saturated flow modeling, *Hydrol. Earth Syst. Sci* **23**, 2897–2914.

Zheng, L., Ma, J., Sun, X., Guo, X., Cheng, Q., Shi, X. 2018. Estimating the root water uptake of surface-irrigated apples using water stable isotopes and the Hydrus-1D model, *Water* **10**, 1624.